Original Research   # *Feature Article*

Heparin-mediated dimerization of follistatin

Ryan G Walker[1], Chandramohan Kattamuri[1], Erich J Goebel[1], Fuming Zhang[2,3], Michal Hammel[4], John A Tainer[5], Robert J Linhardt[2,3] and Thomas B Thompson[1]

[1]Department of Molecular Genetics, Biochemistry and Microbiology, University of Cincinnati, College of Medicine, Cincinnati, Ohio 45267, USA; [2]Department of Chemical and Biological Engineering, Center for Biotechnology and Interdisciplinary Studies, Rensselaer Polytechnic Institute, Troy, New York 12180, USA; [3]Department of Chemistry and Chemical Biology, Center for Biotechnology and Interdisciplinary Studies, Rensselaer Polytechnic Institute, Troy, New York 12180, USA; [4]Molecular Biophysics and Integrated Bioimaging, Lawrence Berkeley National Laboratory, Berkeley, California 94720, USA; [5]Molecular and Cellular Oncology and Cancer Biology, The University of Texas M.D. Anderson Cancer Center, Houston, Texas 77030, USA
Corresponding author: Thomas B Thompson. Email: tom.thompson@uc.edu

Impact statement

The transforming growth factor beta (TGFβ)-signaling pathway is multidimensional and tightly regulated by several mechanisms: from extracellular antagonists and matrix-mediated activation to receptor specificity. Two particular extracellular matrix proteins, heparin and heparan sulfate (HS), bridge antagonism and extracellular matrix-interactions by binding positively charged surfaces on proteins, such as the potent TGFβ antagonist, follistatin. Here, we characterize the interactions between heparin/HS and follistatin, uncovering a heparin/HS chain-length-dependent dimerization of follistatin. This binding localizes the antagonist to the cell surface in a dimeric form, similar to when bound to an antagonist. Heparin/HS-bound follistatin shows altered antagonistic binding to the ligands, myostatin and activin A, suggesting an inverse relation between cell surface availability of follistatin and association rate. This study proposes a mechanism for follistatin dimerization at the cell surface, facilitating follistatin localization and in turn, TGFβ antagonism.

Abstract

Heparin and heparan sulfate (HS) are highly sulfated polysaccharides covalently bound to cell surface proteins, which directly interact with many extracellular proteins, including the transforming growth factor-β (TGFβ) family ligand antagonist, follistatin 288 (FS288). Follistatin neutralizes the TGFβ ligands, myostatin and activin A, by forming a nearly irreversible non-signaling complex by surrounding the ligand and preventing interaction with TGFβ receptors. The FS288-ligand complex has higher affinity than unbound FS288 for heparin/HS, which accelerates ligand internalization and lysosomal degradation; however, limited information is available for how FS288 interactions with heparin affect ligand binding. Using surface plasmon resonance (SPR) we show that preincubation of FS288 with heparin/HS significantly decreased the association kinetics for both myostatin and activin A with seemingly no effect on the dissociation rate. This observation is dependent on the heparin/HS chain length where small chain lengths less than degree of polymerization 10 (dp10) did not alter association rates but chain lengths >dp10 decreased association rates. In an attempt to understand the mechanism for this observation, we uncovered that heparin induced dimerization of follistatin. Consistent with our SPR results, we found that dimerization only occurs with heparin molecules >dp10. Small-angle X-ray scattering of the FS288 heparin complex supports that FS288 adopts a dimeric configuration that is similar to the FS288 dimer in the ligand-bound state. These results indicate that heparin mediates dimerization of FS288 in a chain-length-dependent manner that reduces the ligand association rate, but not the dissociation rate or antagonistic activity of FS288.

Keywords: Follistatin, activin, myostatin (GDF8), heparin, heparan sulfate, transforming growth factor beta

Introduction

The transforming growth factor-β (TGFβ) family of extracellular proteins intimately regulate numerous biological processes including embryonic development, adult tissue maintenance/wound healing, and male/female reproduction. The TGFβ family is composed of more than 30 ligands (subdivided into three subfamilies: activins/inhibins, TGFβs, and bone morphogenetic proteins [BMPs]).

Ligands share a common fold characterized by a cystine knot motif and form covalent dimers that are linked through an intermolecular disulfide bond. Similar in shape to a propeller, the ligand dimer contains two concave and two convex surfaces important for receptor binding. Structural studies have shown that extracellular antagonists effectively block ligand-receptor interactions and neutralize signaling by targeting these same surfaces

(reviewed in Yadin *et al.*[1]). For example, the extracellular antagonist follistatin (FS[2–7]), which binds activin A and myostatin with low nanomolar (nM) affinity,[8–10] completely surrounds the ligand occluding all of the receptor binding sites[11,12] and binds to the ligand with 2:1 stoichiometry (follistatin monomer:ligand dimer).[11–13]

Follistatin was originally identified because of its critical role in regulating the reproductive axis.[2] Follistatin is a 32–35-kDa glycoprotein composed of four domains including an N-terminal domain (ND) followed by three follistatin domains (FSD1, FSD2, and FSD3) where FSD1 contains a linear sequence of basic residues responsible for heparin and HS binding.[14,15] Biochemical studies, along with a co-crystal structure of FSD1 in complex with a small heparin analog, support the role of FSD1 in heparin/HS binding.[16] C-terminal splicing of follistatin can occur to generate various isoforms including FS288 and FS315. The additional residues at the C-terminus of FS315 are acidic and thought to interact with the heparin-binding sequence (HBS) of FSD1, reducing heparin/HS affinity.[17] A related molecule, follistatin-like 3 (FSTL3), contains a similar domain structure without FSD3 but lacks heparin binding.[15]

Binding to HS localizes FS288 to the cell surface thus forming a "canopy" to potentially restrict ligand signaling. Supporting this idea, it was shown that FS288 bound to HS on the cell surface accelerated degradation of activin A therefore providing a mechanism to clear ligands from the extracellular environment.[18] Likewise, in a cell proliferation assay of PA-1 cells, exogenous follistatin inhibited cellular proliferation when cells were treated with exogenous, but not endogenous activin A,[19] suggesting that the interaction between follistatin and the cell surface can differentially mediate ligand signaling. Moreover, we showed that the follistatin:myostatin complex has a higher affinity for heparin than follistatin alone. This indicates that heparin might play a role in regulating not only follistatin but follistatin:ligand complexes.[12] In contrast to FS288, both FS315 and FSTL3 have reduced heparin affinity and are more serum available and thus can function distally from their source of production. Therefore, the follistatin family has emerged with a range of heparin affinity to differentially regulate ligands of the TGFβ family.

The crystal structures of FS288:activin A and FS288:myostatin revealed that the residues in the HBS were not positioned at the ligand interface, implying that heparin/HS binding did not compete with ligand binding.[11,12] However, evidence supports that follistatin in complex with ligand interacts with heparin/HS differently than the unbound follistatin. Initial studies showed that addition of heparin to a preformed activin A:follistatin complex increased the strength of the complex.[20] Furthermore, our recent studies revealed that when follistatin is in complex with the ligand myostatin that the overall affinity of the complex for heparin is dramatically increased for both FS288 and FS315.[12,21] Additionally, it has been shown that the C-terminal tail of FS315 can no longer interact with the HBS when bound to activin A, which explains why FS315 and FS288 activin A complexes have similar affinities for heparin.[17] Taken together, these studies provide evidence that follistatin interacts differently in both the ligand-bound and -unbound states; however, limited studies have reported on how heparin/HS affects follistatin binding to ligands.

Given that FS288 is localized to the cell surface through interactions with heparin/HS, we sought to explore how FS288 bound to heparin/HS would impact ligand binding. Moreover, since formation of the FS288:myostatin complex creates a large electropositive surface, we hypothesized that preloading FS288 with heparin might enhance binding of follistatin to myostatin by dampening electrostatic repulsion. Therefore, we investigated the interaction of heparin-bound follistatin to the ligands myostatin and activin A using surface plasmon resonance (SPR). In contrast to our expectations, results indicate that preloading follistatin with heparin/HS significantly decreases ligand association rates, which is dependent on the size of the heparin molecule. Interestingly, using a combination of biophysical studies, including small-angle X-ray scattering (SAXS),[22] we uncovered that heparin induces dimerization of FS288 in a chain-length-dependent fashion. Our results provide the framework for future studies aimed at defining the structural mechanisms responsible for the observed heparin effects on FS-ligand interactions.

Materials and methods

Production and purification of proteins

Individual proteins (activin A, myostatin, FS288, and FSTL3) were produced and purified as published earlier with some minor modifications.[10–12,23] The purity and quality of all proteins produced were verified using SDS-polyacrylamide gel electrophoresis (PAGE) followed by either Coomassie staining or Western analysis under both reduced and non-reduced conditions. Human activin A was expressed in Chinese hamster ovary (CHO) cells (cell line BA83.6–02) and conditioned medium (CM) was concentrated and dialyzed against 100 mM NaHCO$_3$ pH 7, 150 mM NaCl. The dialyzed material was then applied to a 5 mL HiTrap NHS-activated HP column (GE Lifesciences) coupled to FS288. Activin A was eluted using 50 mM glycine pH 2.5, 1% Triton-100, 150 mM NaCl and subsequently neutralized with 1 M Tris pH 8.0. Dr Se-Jin Lee kindly provided CHO cells over-expressing mouse myostatin. Myostatin CM was concentrated approximately 10-fold using tangential flow and concomitantly buffer exchanged into 50 mM Tris pH 7.4, 500 mM NaCl applied to a Lentil Lectin Sepharose 4B (Amersham Biosciences) column. Myostatin was eluted with the same buffer with the addition of 500 mM methyl mannose. Eluted protein is then dialyzed against 20 mM citrate pH 5.0, 20 mM NaCl and applied to a HiPrep SP FF 16/10 column (GE Lifesciences) and eluted using the same buffer with the addition of 1 M NaCl. The eluted protein was then dialyzed against 20 mM citrate pH 5.0, 20 mM NaCl. Next, the protein was adjusted to 5% acetonitrile, 0.1% trifluoroacetic acid, 4 M guanidinium HCl and applied to a Sepax C4 reverse phase high performance liquid chromatography column. Myostatin was eluted using a linear acetonitrile gradient over 30 column volumes (CV). For follistatin

purification, CHO cells over-expressing FS288 were obtained from Dr Shunichi Shimasaki. CM containing FS288 was adjusted to pH 8.0 and applied to a heparin FF 16/10 column (GE Lifesciences). FS288 was eluted using a linear NaCl gradient over 20 CV. The eluted protein was dialyzed against 25 mM minimal ensemble search (MES) pH 6.5, 150 mM NaCl, applied to a HiPrep SP FF 16/10 column (GE Lifesciences) and eluted using a linear NaCl gradient over 20 CV. At this step in FS288 purification, the protein was used for our initial SPR experiments (see below). For our native-PAGE, size exclusion chromatography (SEC), analytical ultracentrifugation (AUC), and SAXS experiments, purification of FS288 was further refined using a Sepax Proteomix SCX-NP10 4.6 × 250 mm column. FS288 eluent from the HiPrep SP column was diluted 3× in buffer A (2.4 mM Tris, 1.5 mM imidazole, 11.6 mM piperazine pH 6.0). A shallow, linear gradient over 200 CV with buffer B (buffer A with 1 M NaCl, pH 10.5) was run to generate a highly purified sample of FS288 containing a single migrating band determined by SDS-PAGE under non-reducing and reducing conditions visualized by Coomassie staining. FSTL3 was produced as previously described.[24] For quality control, all purified proteins were tested in a luciferase reporter assay as previously described.[10,12,25–27]

Preparation of heparin and HS oligosaccharides

For our analysis, we used either a mixture of heterogeneous heparin ranging in MW of 6–30 kDa with most chains ranging from 17 to 19 kDa obtained from porcine intestinal mucosa (Sigma, #H3393) or size uniformed heparin/HS oligosaccharides. Size uniformed heparin (from dp (degree of polymerization) 4 to dp20) and HS oligosaccharides (from dp6 to dp12) were produced as previously described from controlled partial heparin lyase I treatment of bovine lung heparin or nitrous acid degradation of HS (from porcine intestinal mucosa) followed by size fractionation.[21,28]

Surface plasmon resonance

SPR measurements were performed using a BIAcore 3000 optical sensor system (GE Healthcare, Uppsala, Sweden) and the obtained data were processed with BIAevaluation 4.1 software. Experiments were performed in HBS–EP (10 mM HEPES pH 7.4, 150 mM NaCl, 3 mM EDTA, 0.005% P-20 surfactant [GE Healthcare, Uppsala, Sweden]). Both activin A and myostatin ligands were immobilized on a carboxymethylated dextran matrix (CM5) sensor chip (GE Healthcare, Uppsala, Sweden) in different flow cells using standard amine coupling chemistry according to the manufacturers protocol at 25°C (333 response units [Rus] for activin A and 1611 RUs for myostatin). The remaining activated groups were quenched using 1 M ethanolamine pH 9.0. A reference cell containing no bound protein was used to correct for refractive index changes, non-specific binding, and buffer subtraction. For binding experiments, either FS288 alone or serial dilutions of heparin or HS were premixed with a constant concentration of follistatin diluted in HBS–EP buffer and applied to

the sensor chips for 10 min followed by a 5-min dissociation phase at a flow rate of 20 µL/min. Chip regeneration was accomplished using 15-µL pulse injections of 2 M guanidine HCl at a flow rate of 100 µL/min. As a control, FS288 was reapplied to the chip to determine that the integrity of the chip had not been compromised. The SPR sensorgrams were plotted for each condition using Scrubber 2.0 and Prism GraphPad v5.0a was used to determine IC_{50} values by fitting the data to a sigmoidal dose–response curve using non-linear regression.

Native polyacrylamide gel electrophoresis

For this experiment, purified FS288 (3 µg) alone or preincubated with up to 2.5-fold molar excess heparin or HS chain lengths in 20 mM HEPES pH 7.4, 150 mM NaCl for 15 min, diluted in 2× loading buffer (3 M Tris pH 8.45, 0.1% bromophenol blue, 20% glycerol), and loaded into a 12% polyacrylamide gel buffered at pH 8.8. The gel was run at for 150 min at 100 V at room temp. Protein was visualized with Coomassie stain.

Size exclusion chromatography

SEC was performed on FS288 alone or on FS288 preincubated with molar excess of heparin dp4, dp6, dp10, dp16, and dp20 for use in AUC and SAXS experiments. Complex formation between FS288 and heparin was achieved by adding various prediluted heparin or HS to a solution containing FS288. The sample was then concentrated using Millipore Amicon centrifugal devices (10000 MWCO) for SEC. Purification was done at room temperature using Superdex S75 10/300 GL run in 20 mM HEPES pH 7.4, 1 M NaCl for FS288 alone or 20 mM HEPES pH 7.4, 150 mM NaCl for FS288:heparin/HS complexes. Elution profiles were monitored using UV absorbance at 280 nm. For molecular weight approximation, known molecular weight standards (GE Healthcare) were run using identical conditions (chymotrypsinogen 25 kDa, bovine serum albumin [BSA; 67 kDa]).

Analytical ultracentrifugation sedimentation velocity

Experiments were performed with a Beckman ProteomeLab XL-1 fitted with absorbance optics and a four-hole rotor. Samples and a buffer blank for subtraction were loaded in a two-channel, carbon-filled, epon centerpieces at 48,000 rpm at 20°C. Absorbance was monitored at 230 nm. Interference was monitored for the high protein concentration experiments. Absorbance and interference data were processed using the program Sedfit[29] to determine the sedimentation values and statistics.[30]

Small-angle X-ray scattering

SAXS data were collected at beam line 12-ID-B at the Advanced Photon Source at Argonne National Laboratory and using the SIBYLS beam line mail-in program (Berkeley, CA[31]). FS288 protein and FS288:dp20 complex were purified as described above. Three different concentrations of each sample were analyzed to determine if concentration-dependent effects exist. Data were collected in 20 mM

HEPES pH 7.4, 1000 mM NaCl, 1 mM EDTA for FS288 alone and 20 mM HEPES pH 7.4, 150 mM NaCl, 1 mM EDTA for FS288:dp20 at 10°C. Four exposure times of 0.5, 1, 2, and 5 s were collected. Exposures exhibiting radiation damage were discarded. Buffer matched controls were used for buffer subtraction. ScÅtter (SIBYLS[31–33]) and the ATSAS program suite (EMBL[34]) were used for data analysis. Graphics were generated using UCSF Chimera and Pymol.

FS288 and FS288:dp20 model generation from SAXS data

FS288, chain D from PDB: 3HH2[12] was used as the starting model to generate the FS288 alone models. This model was directly utilized in the AllosMod-FoXS webserver integrated with MODELLER.[35–37] The simulation was allowed to sample all intermediate conformations consistent with the input structure using a temperature scan. To preserve overall protein structure, distance constraints were imposed to maintain disulfide bonds (Cα–Cα; 5 ± 2 Å). A total of 3000 potential monomer models were generated. Next, potential dimer conformations were generated from the initial FS288 monomer and the single best fit (SBF) model from the AllosMod-FoXS run yielding a total of 200 potential dimer conformations using SymmDock (100 from each starting model[38,39]). We then assembled the top 200 models from the AllosMod-FoXS and SymmDock models (200 monomer and 200 dimer models) and performed a MES to identify a SBF model and weighted-average of conformations that best matched our experimental data.[40] To generate the FS288:dp20 models, we started with the two FS288 molecules symmetrically positioned as observed in the FS288:myostatin structure (PDB: 3HH2[12]). The coordinates for myostatin were then removed. Although there is no structure for dp20, a structure for dp18 is available (PDB: 3IRI[41]). Therefore, we positioned heparin dp18 (PDB: 3IRI[41]) over top the known HBS on FS288.[16] This model was then used as the starting model for the AllosMOD-FoXS pipeline. The simulation was allowed to sample all intermediate conformations consistent with the input structure using a temperature scan. Disulfide bonds were constrained to 5 ± 2 Å from Cα–Cα. A total of 30 runs were conducted generating 101 possible structures for each run, yielding both the SBF model and MES models. Graphics were generated using Pymol.

Luciferase reporter assays

Assays were performed using HEK-293-(CAGA)$_{12}$ luciferase reporter cells (initially derived from RRID: CVCL_0045). Here, cells were plated in a 96-well format at a density of 3×10^4 per well and grown for 24 h. At roughly 80% confluence, the growth medium as then removed and replaced with serum free media containing 0.1% BSA and a two-fold titration series of either purified FS288 or FS288:heterogenous heparin complex along with ligand. Ligand concentration was kept constant (0.62 nM). Following an 18-h incubation, the cells were lysed and luminescence was measured using a Synergy H1 Hybrid plate reader (BioTek). Activity data were imported into GraphPad Prism and fit using a non-linear regression with a variable slope to calculate the IC$_{50}$.

Results

Electrostatic potentials of FS288 and FS288:ligand complexes

We previously determined the X-ray crystal structures of FS288 bound to the ligands, myostatin and activin A (Figure 1(a)), where two FS288 molecules symmetrically bind to one ligand dimer.[11,12] Inspection of the electrostatic surface potentials of the FS288:ligand complexes has revealed significant differences between the FS288:myostatin and FS288:activin A complexes. Unlike the FS288:activin A complex, the top and bottom surfaces of the FS288:myostatin complex have highly polar characteristics, where the bottom is electronegative and the top is electropositive (Figure 1(b)). Interestingly, the HBS (aa75-86[15]) of one FS288 molecule forms a continuous basic surface across the bound ligand to the equivalent HBS on the other FS288 molecule (Figure 1(b)). The continuous electropositive surface forms a unique crevice on the surface of the complex, which may represent a larger binding interface for heparin/HS molecules (Figure 1(b)). In support, we have shown that the affinity for heparin is greater when FS288 is in complex with myostatin ($K_d = 0.4$ nM) than FS288 alone ($K_d = 56$ nM[21]) and the complex elutes at a higher ionic strength on a heparin column.[12] This is in stark contrast to the FS288:activin A complex which elutes at a similar ionic strength as FS288 alone,[12] despite a similar affinity ($K_d = 0.47$ nM[21]). These distinctions suggest that fundamental differences may exist in the way FS288 regulates various ligands.

FS288 has different affinity for different ligands. For instance, FS288 has a 10-fold higher affinity for activin A than myostatin ($K_d = 0.5$ nM versus 5.0 nM),[8–10] even though structural studies have revealed that FS288 interacts with myostatin more extensively. However, myostatin is more electropositive than activin and formation of the myostatin FS288 complex results in merging electropositive surfaces from each protein. Thus, an electrostatic barrier might exist that reduces the binding affinity of FS288 for myostatin. Binding results support this idea where affinity differences arise from slower association kinetics for myostatin binding relative to activin, while the dissociation kinetics in each case are nearly irreversible. With this in mind, we speculated that it might be possible to increase the affinity of FS288 for myostatin if FS288 was prebound to heparin/HS to minimize the electrostatic repulsion and thus enhancing the association rate.

Preincubation of FS288 with heparin affects ligand binding

Previous binding experiments have utilized SPR in order to measure the affinity of follistatin for various TGFβ ligands. Therefore, we utilized similar binding experiments to determine what effect preloading follistatin with heparin would have on the affinity of FS288 for myostatin. Here, we incubated FS288 with increasing concentrations of
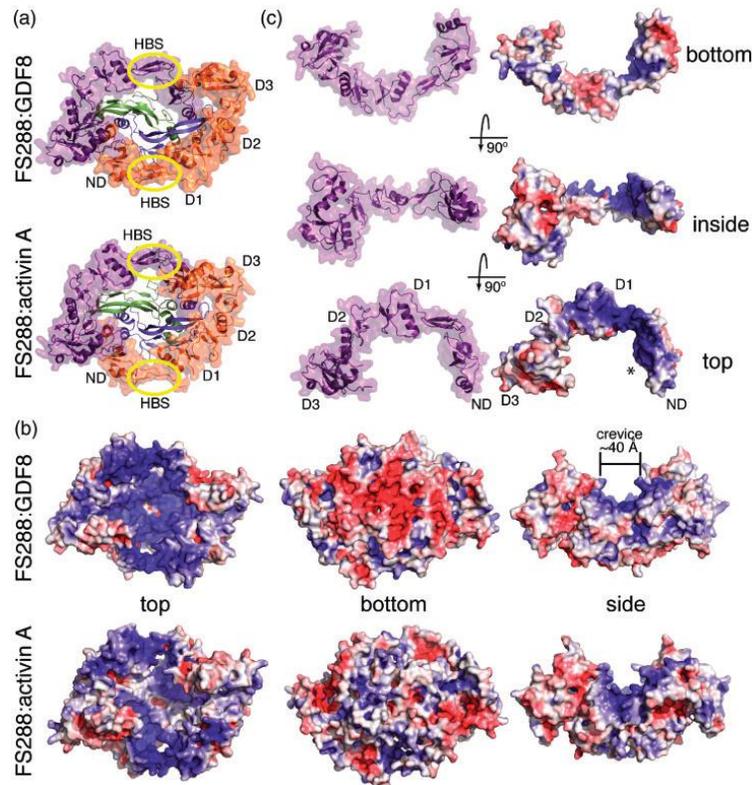
Figure 1. Overview of FS288:ligand structure and heparin-binding location. (a) Structure of FS288:myostatin (PDB: 3HH2[12]) and FS288:activin A (PDB: 2B0U[11]; ligand dimer: green and blue; FS288 monomers: purple and orange; HBS: yellow circle). (b) Electrostatic surface potential comparison between FS288:myostatin and FS288:activin A. Notice the extensive electropositive surface in the FS288:myostatin structure. (c) Ribbon and electrostatic surface view of FS288 monomer. An asterisk marks where the electropositive surface extends beyond the HBS into the ND (asterisks) (blue = basic, red = negative, white = neutral; electrostatic surface potential scale of −5 to 5 k_bT/e_c). (A color version of this figure is available in the online journal.)

heterogeneous heparin (exceeding the K_d between FS288 and heparin: $K_d = 56\,\text{nM}$[21]) and measured binding to myostatin and activin A. Consistent with previous reports, in the absence of heparin, we observed a rapid association and slow dissociation of FS288 with both myostatin and activin A (Figure 2(a) and (b)).[10,21,25] Also consistent with previous reports, the association rate of FS288 for myostatin was qualitatively slower than for activin A. Incubating FS288 with increasing concentrations of heparin resulted in a significant decrease in binding to both myostatin and activin A (Figure 2(a) and (b)). Interestingly, concentrations of heparin less than half the molar equivalents of FS288 had minor effects on ligand binding, whereas higher concentrations of heparin nearly abrogated ligand binding. Additionally, the overall shape of the association curve significantly deviates from a simple Langmuir binding model suggesting that we have observed a more complex binding event (Figure 2(a) and (b)). This effect was readily apparent when the concentration of heparin was half the concentration of FS288. Moreover, the reduction in the overall maximum binding RUs was greater for myostatin than activin A, suggesting that the binding of FS288 to myostatin was more affected by heparin than activin A, likely due to affinity differences between the ligands. Unlike the association phase, the dissociation of FS288 from the ligand did not appear to be

affected by heparin. Therefore, FS288 still forms a very tight and almost irreversible complex in the presence of heparin.

Due to the limitation of our association phase, we did not observe saturation of the ligand binding sites when FS288 was preincubated with heparin (Figure 2(a) and (b)). Therefore, we could not determine if heparin altered the overall binding capacity of the ligand and/or the rate at which FS288 bound to myostatin or activin A. To overcome this, we allowed the association phase to occur for an extended time 2400 s (40 min) followed by the dissociation phase. Again, without heparin, FS288 associated rapidly and within minutes had saturated all ligand-binding sites (Figure 2(c) and (d)). However, in the presence of heparin, we noticed a few distinct differences. Using low concentrations of heparin, binding of FS288 eventually reached similar RUs as compared to FS288 alone. Conversely, at higher concentrations of heparin, we were unable to achieve saturation (Figure 2(c) and (d)). It should also be noted that in all cases heparin significantly disrupted the steady state of follistatin ligand interactions. These results suggest that heparin decreases the rate at which FS288 associates with the ligand and not the total FS288 that can bind.

Since follistatin-like protein 3 (FSTL3) binds both myostatin and activin A with high affinity ($K_d = 1.3\,\text{nM}$ and $K_d = 0.14\,\text{nM}$, respectively[10]) but does not interact with
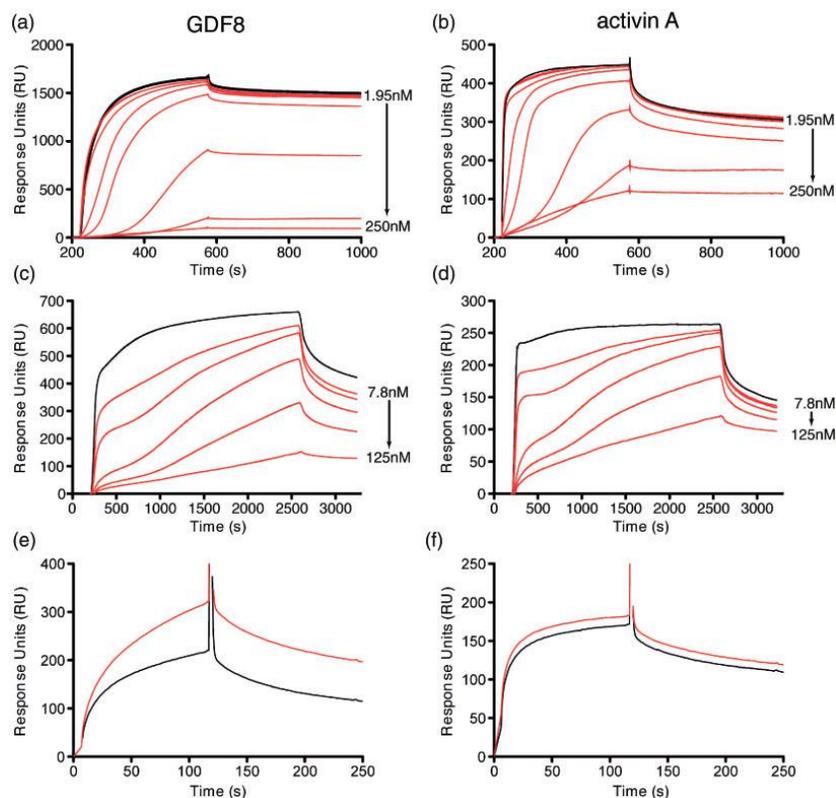
Figure 2. Preincubation of FS288 with heterogeneous heparin alters the association to myostatin and activin A. FS288 (125 nM) passed over myostatin/GDF8 (a) or activin A (b) without heparin (black line). FS288 (125 nM) mixed with 2-fold dilutions of heterogeneous heparin ranging from 250 to 1.95 nM (red lines) and passed over each ligand. Note the changes in the association curve while little to no change can be observed in the dissociation curve. Longer association times and slower flow rates (5 μL/min) are shown for both myostatin/GDF8 (c) and activin A (d). FS288 alone 125 nM (black line) was passed over either myostatin/GDF8 (a) or activin A (b) and achieved saturation readily. FS288 was then held at a constant concentration (125 nM) and preincubated with various concentrations of heterogeneous heparin (7.81–125 nM; red lines) and passed over either ligand. Even at the highest concentrations of heparin, FS288 continues to accumulate mass indicating continual saturation was not achieved. FSTL3 (125 nM) was passed over myostatin/GDF8 (e) or activin A (f) without heparin (black line). FSTL3 (125 nM) mixed with a 10-fold molar excess of heterogeneous heparin and passed over each ligand. (A color version of this figure is available in the online journal.)

heparin,[15] we performed a similar SPR experiment where we preincubated FSTL3 with heparin. Similar to previous reports, FSTL3 bound to both myostatin and activin A (Figure 2(e) and (f) [10,25]). Preincubation of FSTL3 with heterogeneous heparin at a 10-fold molar excess had no effect on FSTL3 binding to activin A and actually potentiated myostatin binding (Figure 2(e) and (f)). It should also be noted that heparin did not associate with either ligand. This is consistent with the notion that, unlike BMP ligands,[42,43] myostatin and activin A do not interact with heparin or the cell surface. Taken together, these results demonstrate that the heparin effects observed with FS288 are a direct result of heparin:FS288 interactions and not non-specific interactions.

Heparin/HS chain length differentially affects FS288 ligand binding

Heparin and HS are synthesized in a variety of molecular weights corresponding to not only chain length but also glycosaminoglycan composition differences. These differences can affect the affinity for the targets to

which they bind (reviewed in Capila and Linhardt[44] and Bishop *et al.*[45]). Previously, we showed that the FS288: ligand complex has preferences for chain lengths of heparin greater than dp10.[21] Since the experiments above were conducted with heterogeneous heparin, we next wanted to determine if the slower association of FS288 with ligands in the presence of heparin was dependent on heparin dp (e.g. chain length). Therefore, we incubated FS288 with highly pure, size uniformed heparins and HS of various lengths and performed SPR binding analysis. FS288 [50 nM] was preincubated with saturating concentrations of the various heparins [1 μM] and analyzed for either myostatin or activin A binding (Figure 3(a) and (b)). Our results indicate a clear size dependence on heparin chain length where longer chain lengths of heparin (≥dp10) decreased FS288 association similarly for both myostatin and activin A. Interestingly, we observed minimal to no inhibition with dp4 and moderate inhibition using dp6 and dp8 suggesting that there is a minimal length/size requirement for heparin to alter the binding of FS288 with its ligands. Similar to the heterogeneous heparin, the dissociation rate was relatively
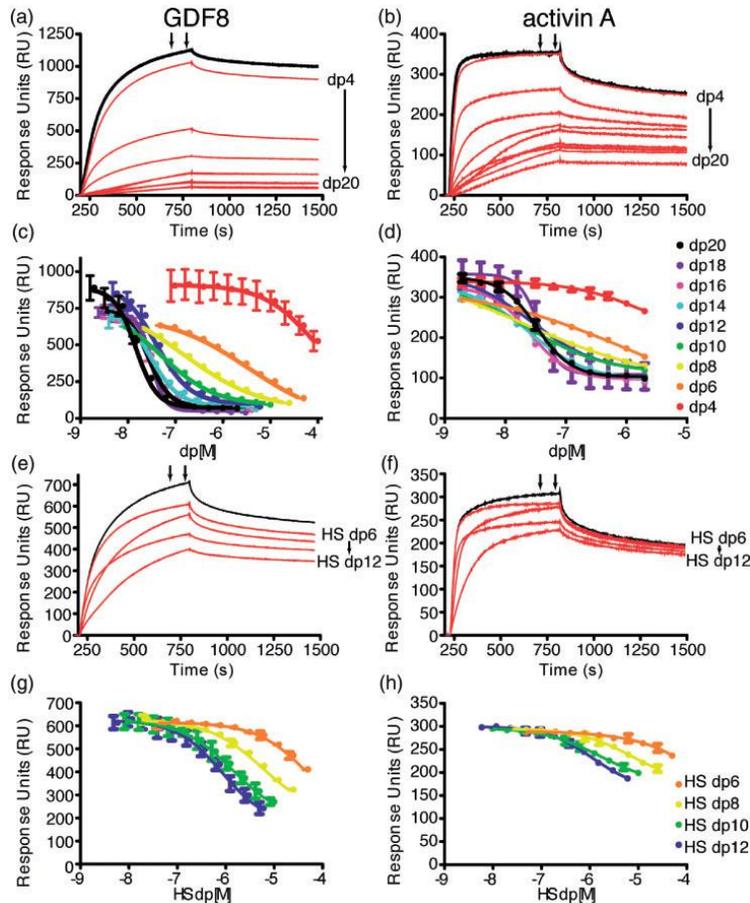
Figure 3. Altered ligand association is dependent on heparin/HS chain length. FS288 at a concentration of 50 nM was passed over myostatin/GDF8 (A, E) or activin A (B, F) without heparin (black line). FS288 was then held constant at 50 nM and mixed with 1 μM of highly pure, chemically defined heparin of various chain lengths ranging from dp4 to dp20 (A, B; red lines) and passed over each ligand. Notice the dramatic changes in the association as the chain length increases from dp4 to dp20. For heparan sulfate, FS288 was held constant at 50 nM and mixed with 1 μM highly pure heparan sulfate of various chain lengths ranging from dp6 to dp12 (red lines) and passed over myostatin/GDF8 (e) and activin A (f). Notice that similar chain lengths of heparan sulfate did not affect FS288 to the same degree as heparin. In (C, D) and (G, H), the relative maximum binding (RU) achieved (black arrows, A, B and E, F) when 50 nM FS288 was preincubated with various chain lengths and concentrations of heparin and heparan sulfate and passed over either myostatin or activin A. IC_{50} values were determined by titrating increasing amounts of heparin and fitting the curves to a sigmoidal dose–response curve using non-linear regression in Prism GraphPad v5.0a. Error bars represent standard deviation from the average of the two black arrows shown in (A, B) and (E, F). (A color version of this figure is available in the online journal.)

unaltered by the presence of various heparin sizes and remained nearly irreversible.

We next wanted to determine if there was a difference in ligand binding when FS288 was preincubated with HS as compared to heparin and, if binding in the presence of HS also displayed a size dependence. Aside from glycosoaminoglycan composition differences, HS has a lower content of sulfate modification than heparin thus resulting in a slightly less negative molecule. Indeed, both HS and heparin altered the association of FS288 with both ligands, although the effect was much less pronounced for HS (Figure 3(e) and (f)). Though less dramatic than heparin, there was a dependence on the chain length of HS. Here, our results show that HS dp12 and dp10 altered FS288 association greater than dp8 and dp6 chain lengths for both myostatin and activin A (Figure 3(e) and (f)). Again, there was minimal difference in the dissociation of FS288 when HS was present (Figure 3(e) and (f)).

Heparin is more effective at altering FS288 association to myostatin and activin a than HS

Since the above experiments were performed with saturating concentrations of heparin or HS, we next wanted to determine an apparent half maximal inhibition (IC_{50}) value for the various chain lengths of heparin/HS (Figure 3(c), (d), (g), and (h) and Tables 1 and 2). In this experiment, FS288 was held at a constant concentration of 125 nM and then preincubated with heparin or HS at various concentrations. At the conclusion of the association phase, the peak RU was recorded as shown by the black arrows in Figure 3. The two arrows were set 100 s apart and the average of the two arrows was plotted against concentration to generate an apparent IC_{50} value for each heparin or HS chain length. Using this analysis, we determined IC_{50} values for heparin chain lengths greater than dp8 for both myostatin and activin A (Table 1). For chain lengths $\geq$dp12, the measured IC_{50} values exhibited a narrow range of

Table 1 IC$_{50}$ values for heparin inhibition of ligand binding.

Ligand	Heparin	IC50 [M]	IC50 (95% CI)
Myostatin	dp20	1.8×10^{-8}	$1.5–2.1 \times 10^{-8}$
	dp18	3.8×10^{-8}	$3.4–4.3 \times 10^{-8}$
	dp16	3.6×10^{-8}	$2.9–4.0 \times 10^{-8}$
	dp14	3.8×10^{-8}	$2.9–5.0 \times 10^{-8}$
	dp12	4.7×10^{-8}	$3.4–6.7 \times 10^{-8}$
	dp10	6.6×10^{-8}	$5.3–8.4 \times 10^{-8}$
	dp8	1.8×10^{-7}	$1.2–2.6 \times 10^{-7}$
	dp6	4.3×10^{-6}	$3.2–5.7 \times 10^{-6}$
	dp4	NC ($>1.0 \times 10^{-6}$)[a]	NC
Activin A	dp20	3.3×10^{-8}	$3.0–3.6 \times 10^{-8}$
	dp18	5.4×10^{-8}	$3.8–7.5 \times 10^{-8}$
	dp16	5.1×10^{-8}	$4.2–6.1 \times 10^{-8}$
	dp14	6.2×10^{-8}	$4.6–8.3 \times 10^{-8}$
	dp12	8.3×10^{-8}	$5.9–11.6 \times 10^{-8}$
	dp10	1.2×10^{-7}	$9.4–14.1 \times 10^{-8}$
	dp8	2.7×10^{-7}	$1.4–5.4 \times 10^{-8}$
	dp6	NC ($>2.8 \times 10^{-5}$)	NC
	dp4	NC ($>8.9 \times 10^{-5}$)	NC

[a]NC, not calculable.

Table 2. IC$_{50}$ values for HS inhibition of ligand binding.

Ligand	HS	IC$_{50}$ [M]	IC$_{50}$ (95% CI)
Myostatin	dp12	1.0×10^{-6}	$4.8–21.6 \times 10^{-7}$
	dp10	1.8×10^{-6}	$6.4–49.0 \times 10^{-7}$
	dp8	7.2×10^{-6}	$3.9–13.4 \times 10^{-6}$
	dp6	7.4×10^{-6}	$7.0–791 \times 10^{-6}$
Activin A	dp12	1.2×10^{-6}	$6.6–20.4 \times 10^{-7}$
	dp10	1.6×10^{-6}	$7.8–34.2 \times 10^{-7}$
	dp8	7.7×10^{-6}	$2.5–23.4 \times 10^{-5}$
	dp6	NC (>0.7)[a]	NC

[a]NC, not calculable.

values from 1.8×10^{-8} to 8.3×10^{-8} M and showed similar results for both activin A and myostatin (Table 1). We were unable to determine an IC$_{50}$ value for chain lengths less than dp8 due to the more limited effect on binding (Figure 3(c) and (d) and Table 1). Similarly, we were unable to determine reliable IC$_{50}$ values for the HS chain lengths at the concentrations tested (Figure 3(g) and (h) and Table 2). Taken together, our results suggest that heparin is more effective than HS and that heparin sizes of dp12 or larger are the most effective for impacting the association of FS288 to the ligands myostatin and activin A.

Heparin induced oligomerization of FS288

At the onset of our study, our initial hypothesis was that preincubation of FS288 with heparin or HS would improve affinity for myostatin compared to FS288 alone. However, our SPR results clearly refute this hypothesis. One potential explanation for this outcome is that preincubation of FS288 with heparin or HS results in the formation of a FS288:heparin or FS288:HS complex that masks the ligand-binding epitope of FS288. With this in mind, we wanted to set out to characterize the complex of FS288 with heparin or HS. First, we assessed the migration of FS288 alone and preincubated with a molar excess of various heparin/HS chain lengths using basic pH native-PAGE (Figure 4(a) and (b)).

FS288 alone did not significantly migrate into the gel under these conditions, likely due to a theoretically high isoelectric point (p$I \sim 8.2$). However, preincubation of FS288 with heparin or HS resulted in a significant shift in migration indicative of complex formation between FS288 and the corresponding heparin or HS (Figure 4(a) and (b)). Interestingly, a distinct migration profile was observed for each heparin and HS chain length indicative of complex formation between FS288 and heparin or HS. For heparin, migration of FS288 with the smaller chain lengths ($\leq$dp12) often resulted in two or more distinct bands (compare lanes 2–6 in Figure 4(a), left) indicative of a heterogeneous sample. However, preincubation with larger chain lengths resulted in resolution of one distinct band suggesting formation of homogeneous complex (compare lanes 7–10 in Figure 4(a)). In contrast, all chain lengths tested for HS resulted in two or more distinct bands, thus resembling the migration pattern observed for smaller heparin chain lengths (Figure 4(b)).

Given the distinct native-PAGE migration profiles observed for the various FS288:heparin/HS mixtures, we wanted to determine if these differences were a result of different oligomerization states. To address this possibility, we compared the complexes between FS288 and various chain lengths of heparin or HS using SEC (Figure 4(c) and (e)) and AUC (Figure 4(d) and (f)). First, we applied FS288 alone to a Superdex S75 10/300 SEC column and compared it to sizing standards of known mass (Figure 4(c) and (e)). FS288 eluted just before the 25 kDa which is close to the its predicted MW ($\sim$32 kDa). It should be noted that inclusion of 1 M NaCl in the running buffer was required to prevent loss of FS288 protein due to non-specific adherence of FS288 to the Superdex resin. However, to determine the retention volume of various FS288:heparin or HS complexes, we reduced the concentration to 150 mM NaCl. Interestingly, when FS288 was mixed with a molar excess of heparin dp4 and dp6, only a small fraction of the sample was recovered (Figure 4(b)) suggesting loss of the protein to the column. In contrast, samples composed of FS288 and larger heparin chain lengths (dp10, dp16, and dp20) readily eluted from the column. Unexpectedly, the retention volume for these complexes shifted $\sim$2 mL to left of where FS288 alone eluted and aligned near the 67 kDa sizing standard (Figure 4(c)) suggesting a significant increase in the size or change in shape of the migrating species. Although less pronounced, preincubation of FS288 with HS dp12 resulted in a leftward shift in retention volume compared to FS288 alone (Figure 4(e)). In addition, preincubation of FS288 with heterogeneous mixture of HS (LMWHS) resulted in an even further shift suggesting formation of higher order oligomers (Figure 4(e)).

Next, we turned to AUC-sedimentation velocity (SV) to clarify our native-PAGE and SEC results. As expected, SV showed that our FS288 (0.1 mg/mL) sample contained a single species with a sedimentation coefficient of 2.5 S and frictional ratio (f/f_o) of 1.4 (Figure 4(d) and Table 3), whereas at higher concentration (2.5 mg/mL), self-association of FS288 started to appear. Similar values were determined when the experiment was performed in the presence of 1 M NaCl (Figure 4(d) and Table 3), which
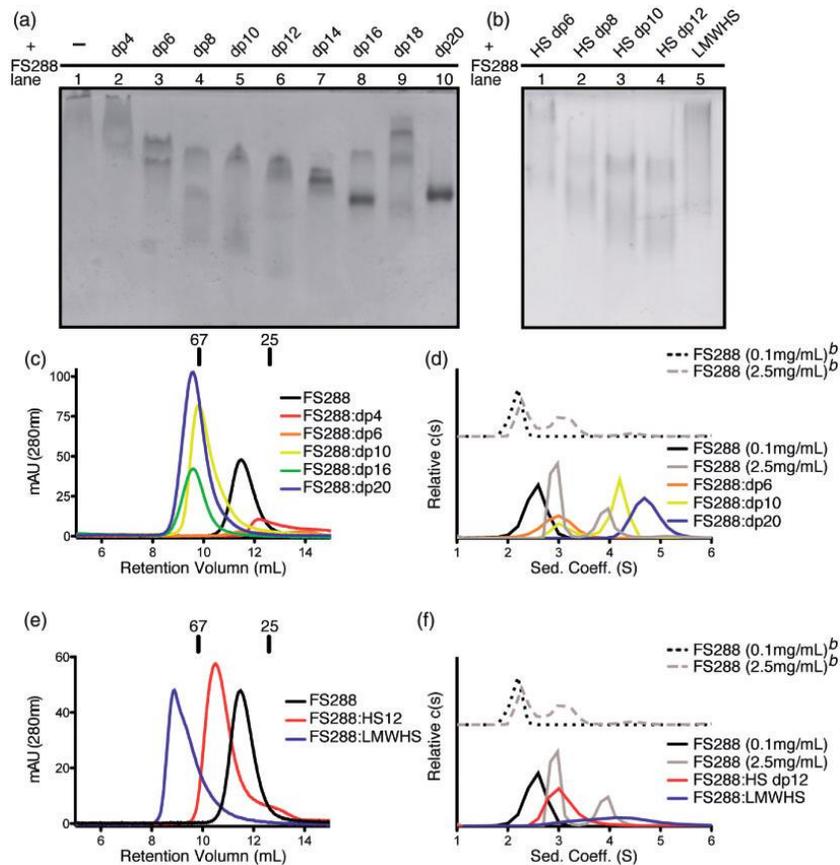
Figure 4. Heparin-mediated dimerization of FS288. Basic native-PAGE of FS288 and heparin (a) or heparan sulfate (b) complexes. Three micrograms of FS288 was mixed with ≥2-fold molar excess of heparin or heparan sulfate chains. (C, E) Size exclusion chromatography results for the FS288 alone and FS288:heparin (c) or FS288:heparan sulfate (e) complexes. Sizing standards are shown above each graph. (D, F) Sedimentation velocity results for the FS288 alone and FS288:heparin (d) or FS288:heparan sulfate (f) complexes. See also Table 3. (A color version of this figure is available in the online journal.)

Table 3. Sedimentation velocity and statistics for FS288 and FS288:heparin/HS complexes.

Protein	mg/mL	$c(s)$[a]	f/f_o	RMSD	MW (kDa)
FS288	0.1	2.5	1.4	0.007	33
FS288[b]	0.1	2.2	1.4	0.009	33
FS288	2.5	2.9 (55%); 3.9 (30%)	1.1	0.015	28; 44
FS288[b]	2.5	2.3 (42%); 3.1 (38%); 4.4 (6%)	1.5	0.032	31; 47; 81
FS288:dp6	0.1	3.0	1.2	0.007	38
FS288:dp10	0.1	3.1 (24%); 4.2 (76%)	1.2	0.005	38; 59
FS288:dp20	0.1	4.7	1.2	0.005	69
FS288:HS12	0.1	3.1	1.2	0.005	37
FS288:HSLMW	0.1	4.2	1.3	0.007	62

Note: MW calculations for each peak.
[a]Values in parentheses are percentage of total signal from sedimenting particles.
[b]Performed in buffer containing 1 M NaCl.

together suggest that the NaCl did not significantly affect the protein oligomeric status or shape (Table 3). Importantly, the apparent molecular mass was consistent with the theoretical mass and mass spectrometry results (Table 3). A single peak at 3.5 S with an apparent molecular mass of 38 kDa was observed when FS288 was mixed with heparin dp6 (Figure 4(d)) suggesting that FS288 had formed a monodisperse complex with dp6 and adopted a globular shape ($f/f_o = 1.2$). However, two peaks were observed when FS288 was mixed with dp10, indicative of a heterogeneous sample (Figure 4(d) and Table 3). The first peak had a similar sedimentation coefficient and apparent molecular mass as the FS288:dp6 sample while the additional peak at 4.2 S and apparent molecular mass of 59 kDa (Table 3) suggesting formation of a dimer species. Finally, addition of dp20 resulted in a single peak at 4.7 S with an
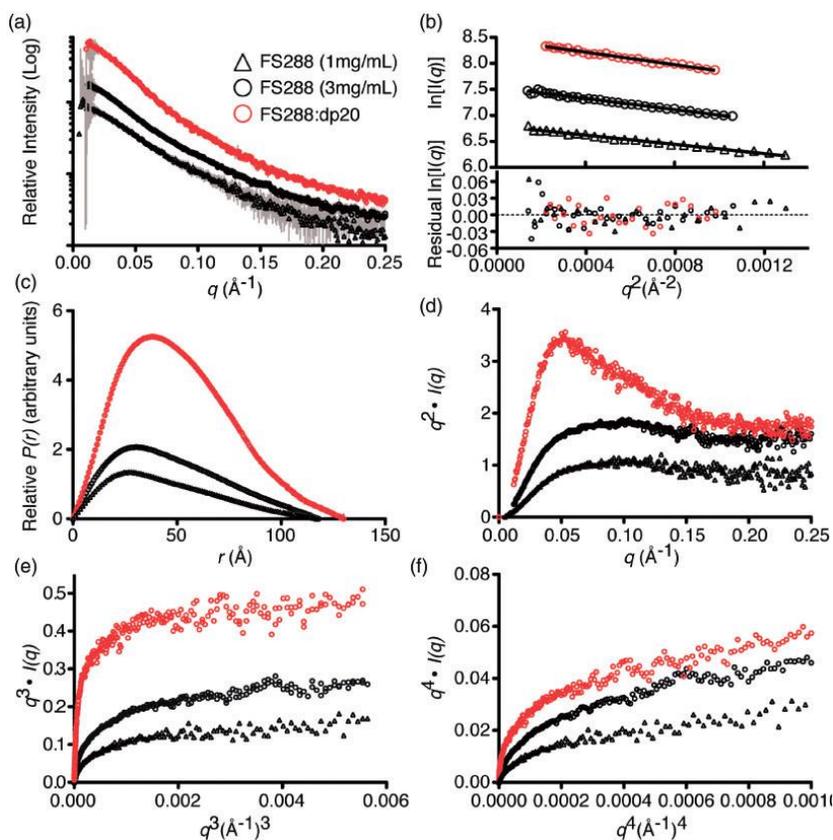
Figure 5. SAXS analysis on FS288 and the FS288:dp20 complex. (a) Intensity distribution of the SAXS scattering function for FS288 alone at 1 mg/mL (open black triangles) and 3 mg/mL (open black circles) and the FS288:dp20 complex (open red circles). (b) Gunier plot for FS288 alone and the FS288:dp20 complex showing a linear, unbiased distribution. Residuals are shown below each plot. (c) Pairwise distribution function for FS288 alone and the FS288:dp20 complex. (D–F) Flexibility plots for FS288 alone and the FS288:dp20 complex: (d) $q^2 \cdot I(q)$ versus $q^2(\text{Å}^{-1})^2$, (e) $q^3 \cdot I(q)$ versus $q^3(\text{Å}^{-1})^3$, and (f) $q4 \cdot I(q)$ versus $q4(\text{Å}^{-1})^4$. See also Table 4. (A color version of this figure is available in the online journal.)

apparent molecular mass of 69 kDa (Figure 4(d) and Table 3). Interestingly, incubation of FS288 with HS dp12 resulted in a similar sedimentation profile as FS288:dp6, suggesting FS288 formed a complex with HS dp12 (Figure 4(f) and Table 3). In contrast to FS288:dp10, incubation of FS288 with HS dp12 did not result in two distinct species. Incubation of FS288 with LMWHS resulted in a poorly resolved peak ranging from ∼2 to 6 S with the peak maxima at 4.2 S. Despite the poor resolution, these results are suggestive that the longer chain lengths of HS within this sample likely facilitate formation of oligomeric species. Taken together, these results suggest that dimerization of FS288 can be mediated by heparin in a chain-length-dependent fashion. Although it is clear the HS can bind to FS288, our results indicate that longer chain lengths of HS than tested here are likely to be required to mediate dimerization of FS288.

SAXS analysis of FS288 and the FS288:dp20 complex

SAXS data were collected on equal protein concentrations of FS288 alone and FS288:dp20 that had been subjected to SEC prior to data collection. The SAXS scattering profiles for FS288 and the FS288:dp20 complex are shown in

Figure 5(a), along with the corresponding analysis in Table 4. Samples were well behaved in solution and did not show evidence of interparticle repulsion or aggregation over multiple protein concentrations (Figure 5(a) and Table 4). Therefore, the SAXS data were further analyzed and comparisons with FS288 alone to FS288:dp20 were made.

We determined that the FS288:dp20 complex has a slightly larger R_g than FS288 alone (Figure 5(b) and Table 4). Similarly, the maximum particle distance (D_{max}) derived from the pairwise distance–distribution function ($P(r)$) curve revealed that FS288:dp20 complex is only slightly longer than FS288 alone (Figure 5(c) and Table 4). However, based on the shape of the shape of the $P(r)$ curve, FS288 adopts an extended conformation, whereas the FS288:dp20 complex is more globular in nature (Figure 5(c)). Further, transformation of the SAXS data indicates that both FS288 and the FS228:dp20 complex are inherently flexible as indicated by the plateau in the $q^3 I(q)$ versus $q^3(\text{Å}^{-1})^3$ plot (Figure 5(e)) compared to a lack of plateau in either the $q^2 I(q)$ versus $q^2(\text{Å}^{-1})^2$ or $q4 I(q)$ versus $q4(\text{Å}^{-1})^4$ plots which would indicate unfolded or rigid structures, respectively (Figure 5(d) and (f)).[46] We also determined that FS288 alone and the FS288:dp20 complex are flexible in solution.

Table 4. SAXS-derived analysis of FS288 and FS288:dp20 complex.

Protein	mg/mL	R_g (Gunier)[a]	R_g (P(r))	I(0) (Gunier)	D_{max} (Å)	Volume (Å^3)	MW (kDa)
FS288	3	39.4 ± 1.1	37.6 ± 0.1	1900	~120	141,000	37
	2	39.4 ± 2.7	36.3 ± 0.3	1100	~120	159,000	46
	1	34.7 ± 2.3	33.9 ± 0.2	570	~100	107,000	56
FS288:dp20	3	44.9 ± 0.6	42.1 ± 0.1	6400	~130	232,000	69
	2	44.0 ± 1.2	41.1 ± 0.1	3900	~130	198,000	83
	1	40.1 ± 1.7	40.5 ± 0.4	1800	~130	174,000	99
FS288:dp20 (averaged)		42.6 ± 2.1	39.0 ± 0.3		~130	175,000	72
FoXS							
FS288[b]		30.6	–	–	84 (140)[c]	31,810	31.6

[a]R_g, radius of gyration.

.
[b]Theoretical values calculated from PDB: 3HH2, chain D.
[c]Value in parentheses indicates theoretical D_{max} for extended FS288 conformation.

Consistent with our previous findings, the molecular mass derived from the SAXS data places the FS288:dp20 complex within 69–99 kDa range depending on the concentration assessed strongly suggesting that the complex is composed of at least two FS288 molecules and one dp20 molecule. Interestingly, the apparent molecular weight for FS288 ranged from 37 to 56 kDa. Together with the minor fluctuations in calculated R_g (compare the data for FS288 alone at the 1 mg/mL versus 3 mg/mL in Figure 5 and Table 3) and our AUC data, it is likely that FS288 likely self-associates in a concentration-dependent fashion.

SAXS-derived models of FS288 and FS288:dp20 complex

First, we compared FS288 (PDB: 3HH2; chain D[12]) to the SAXS data using FoXS.[36,47] At the low concentration of FS288, our experimental data closely match the theoretical scattering profile FS288 as indicated by a $\chi = 0.29$ (Figure 6 (a)), whereas the experimental data for the 3 mg/mL sample significantly deviate from the crystal structure ($\chi = 2.02$; Figure 6(b)). The theoretical scattering profile for FS288 deviates even further from the experimental FS288:dp20 SAXS data ($\chi = 5.89$; Figure 5(c)). In order to obtain a more representative model for each of these scattering profiles, we generated a SBF model and a representative ensemble of potential models that best represented our experimental data using the AllosMod-FoXS[37,47] and SymmDock[38] webservers (see materials and methods).

The resultant SBF model ($\chi = 0.35$) for FS288 at 1 mg/mL was determined to be a monomer and is shown in Figure 6 (a). Only a modest improvement in the overall fit ($\chi = 0.29$) was observed using a MES,[40] which included a contribution from the SBF model (45%) and an additional dimer model (55%; Figure 6(a)). For the 3 mg/mL FS288 sample, we were able to achieve a significant improvement in the overall fit using MES ($\chi = 0.69$) over the SBF model ($\chi = 1.06$; Figure 6(b)). Consistent with our earlier assessment, a variety of FS288 dimer configurations best represented the data with only a minor contribution from FS288 monomers (Figure 6(b)). Similarly, MES models improved the overall fit compared to the SBF model alone

($\chi = 1.67$ versus $\chi = 1.48$, respectively; Figure 6(c)). Overall, the FS288:dp20 models are quite similar where heparin bridges two FS288 molecules oriented in an anti-parallel fashion. The primary divergence between the models is the proximity between the two FS288 molecules. Although these models fit the experimental data quite nicely, it is clear that our theoretical models do not account for all possible conformations or partial conformations. Higher resolution or additional restraints based on experimental evidence are likely needed to accurately represent the experimental data.

FS288 and FS288:heparin complexes similarly antagonize GDF8 and activin A in vitro

Given that heparin binding to follistatin yields a dimer, we wanted to compare the inhibitory capacity of FS288:heterogenous heparin to that of unbound, monomeric FS288. Here, a luciferase reporter assay was utilized with HEK293 cells, where the smad2/3 responsive (CAGA)$_{12}$ luciferase reporter was stably transfected. Titration of both unbound FS288 and FS288:heterogenous heparin against a constant concentration of exogenous GDF8 resulted in similar inhibitory effects (Figure 7(a)). Resultant IC50 values were 0.79 and 0.88 nM, respectively. Similar inhibition was also observed during FS288 titration against activin A, yielding IC50 values of 0.25 nM for FS288 and 0.45 nM for FS288:dp20 (Figure 7(b)). Overall, in this *in vitro* experiment, heparin binding and dimer formation does not significantly affect the inhibitory capacity of FS288.

Discussion

Extracellular modulation of TGFβ ligand signaling occurs through a combination of mechanisms, including ligand latency/activation, differential receptor utilization/specificity, and the presence of ligand antagonists. However, only a number of studies have investigated the role of heparin/HS in these various mechanisms.[12,15,21,48,49] More specifically, there are limited studies characterizing the interactions between antagonists and heparin/HS.[12,15,16,21] The results of the present study build upon
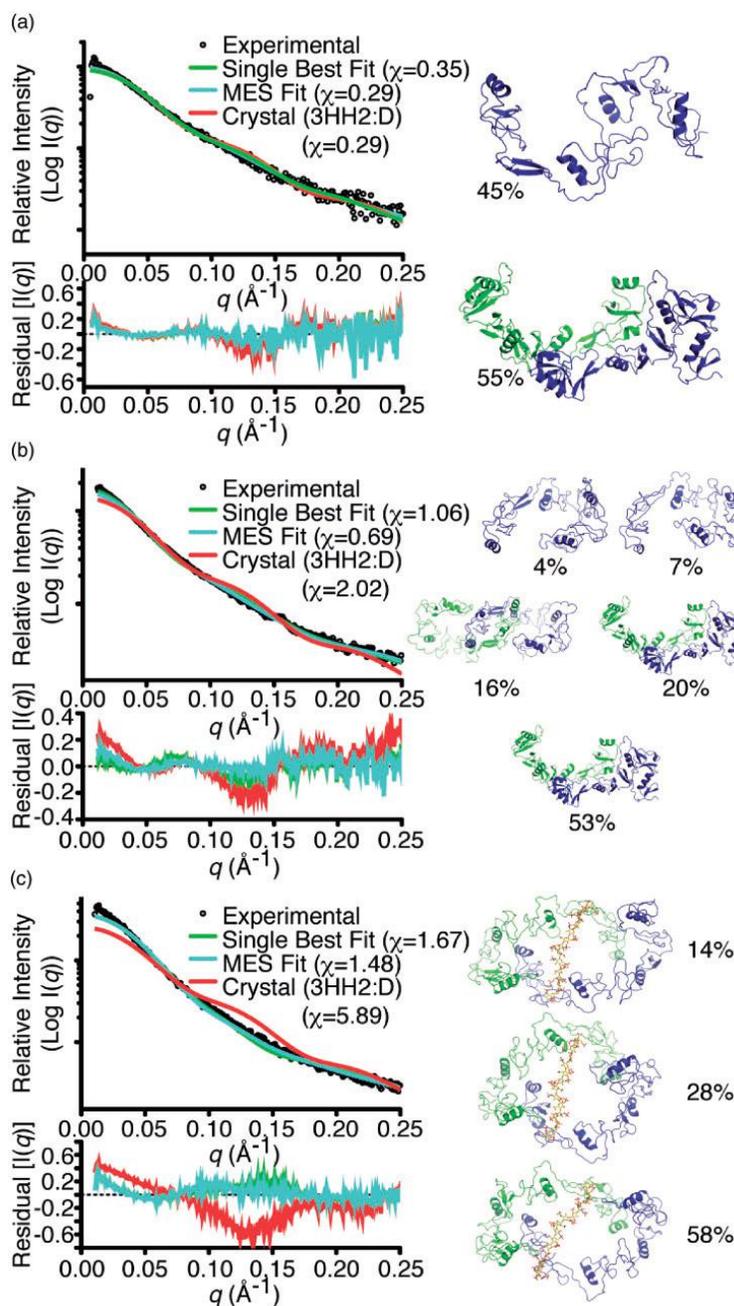
Figure 6. Generation of FS288 and FS288:dp20 models and comparison to SAXS data. AllosMod-FoXS results for FS288 alone based on SAXS data collected at 1 mg/mL (a) and 3 mg/mL (b) and the FS288:dp20 complex (c). Theoretical scattering profiles determined by FoXS are shown superimposed over the experimental SAXS data with the Chi distribution shown in parentheses. The residuals for each profile compared to the experimental data are shown below each graph. The corresponding MES-derived models are shown to the right of each graph. The value in parentheses represents the total scattering contribution of that model for the MES weight-averaged theoretical scattering profile. FS288 models are shown in blue and green. Heparin dp20 model is shown in yellow. (A color version of this figure is available in the online journal.)

previous knowledge of follistatin and its interaction with heparin/HS and examines the impact of heparin/HS association with follistatin prior to ligand binding. Here, we have determined that prebinding FS288 with heparin significantly impairs the association with myostatin and activin A and that this effect is less pronounced with HS. Further, we show that heparin potentiates dimerization

of FS288 in a chain-length-dependent fashion and similarly, HS does so less effectively. Finally, we present theoretical models of the FS288 and heparin dp20 complex based on SAXS.

While FS288 effectively antagonizes both myostatin and activin A, the crystal structure of FS288 bound to myostatin indicated a convergence of electropositive surfaces.
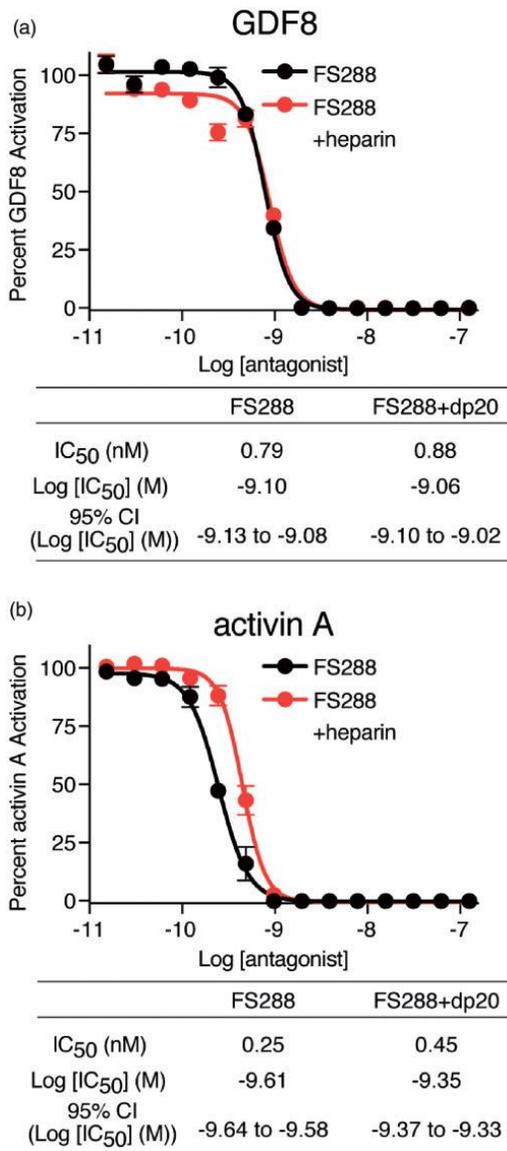
Figure 7. FS288 and FS288:heparin antagonism of GDF8 and activin A. Inhibition curves (CAGA-luciferase) following titration of either FS288 (black) or FS288:heterogenous heparin (red) against a constant concentration of purified ligand: myostatin/GDF8 (a) or activin A (b). IC_{50} values were determined by fitting the curves using non-linear regression in Prism GraphPad v5.0a. Each data point represents the mean $\pm$ SD of triplicate experiments measuring relative luminescence units (RLU), represented by a percentage of uninhibited signaling of the respective ligand. (A color version of this figure is available in the online journal.)

While FS288 primarily utilizes hydrophobic interactions to support a high-affinity interaction with both myostatin and activin, it was interesting that the top and bottom surfaces of the FS288:myostatin complex exhibit highly polar and oppositely charged characteristics. Given the more electropositive nature of myostatin, an electrostatic barrier may result in some repulsion, and therefore weaker interactions. We thought that binding of follistatin by heparin may serve to mediate these effects.

To test this idea, we preincubated FS288 with heparin with the intent of minimizing the electrostatic contribution of residues in the HBS of FS. However, our results unexpectedly show that heparin/HS significantly decreases the association rate of FS288 to myostatin. Furthermore, this observation appears to be ligand independent as binding to both myostatin and activin A is reduced. We also determined that this observation is highly dependent on the size of heparin with a strong preference for heparin sizes of dp12 or greater.

The dependence on chain length could be a result of two possibilities (which are not mutually exclusive): (1) the longer chain lengths (due to increased size and charge) have a higher affinity for FS288 and are thus more effective and (2) the larger heparin molecules interact additional surfaces of follistatin located outside the HBS of follistatin that are also important ligand binding. Upon closer inspection of the electrostatic surface potential of FS288 in the absence of a ligand, we noticed that the electropositive patch extends beyond FSD1 and into the ND (Figure 1(c)). This electropositive patch includes the canonical HBS, plus additional residues in the ND at the ligand interface that may contribute to heparin/HS binding; e.g. Arg6 of follistatin, which interacts, with the N-terminus of myostatin.[12]

The notion of an additional binding surface is also supported by our previous work where we showed that FS288 has higher affinity for longer heparin chains in a competition assay.[21] For example, a dp20 molecule is approximately ~80 Å which not only permits interaction with the known heparin-binding site, but also allows it to potentially bind additional sites along the length of the FS288 molecule. Therefore, the altered association rate may be a result of heparin occluding the surfaces of FS288 that would normally bind to the ligand in addition to the HBS. Specifically, FS288 basic residues Arg6, Lys9, Arg12, Lys18, and Lys23 all reside in close proximity within the internal surface of the ND and potentially could bind heparin. In fact, Arg6 mediates an important salt bridge with myostatin Asp1 when in complex.[12] Thus, occlusion of these residues could have a significant impact on ligand binding.

Another possibility is that the longer chain heparins are imposing physical constraints that slow binding. Since the domains of FS288 must adopt curvature to "wrap" around the ligand, heparin binding might reduce the relative flexibility of the domains. Further, it should be noted the inhibitory effects observed with the longer chain lengths of heparin cannot be recapitulated with simply increasing the concentration of smaller chain lengths. A continuous length of heparin is necessary for inhibition, whereas binding by multiple smaller chain lengths will not result in this same inhibitory effect. This suggests that a specific interaction between follistatin and long chain lengths of heparin is necessary for the observed effect. Supporting this idea, longer chain lengths of heparin mediate dimerization of FS288. Though at this point we cannot determine what is responsible for the altered association profile, we speculate that dimerization induced by longer chain lengths of heparin is responsible for the altered association of FS288 with myostatin and activin A. This is supported in that the shorter chain lengths, which bind, but do not facilitate

dimerization of FS288, do not significantly impair FS288 association with myostatin or activin A. Nonetheless, additional biophysical and structural characterization will be required to clarify this observation.

When comparing similar chain lengths, we showed that heparin is much more effective than HS at altering FS288 ligand binding. Though heparin and HS are similar, there exist fundamental differences in their sulfation patterns. Heparin contains more sulfate groups, which likely explains why FS288 has a higher affinity for heparin over HS, and also may explain why heparin is more effective at decreasing ligand binding compared to HS. HS is the predominant glycosaminoglycan present on the cellular surface and undergoes extensive modification based on cellular environmental cues and requirements (reviewed in Bishop *et al.*[45]). Although additional studies are needed to identify the biological significance of heparin-mediated dimerization of FS288, our *in vitro* experiments revealed similar inhibitory activity of dimer and monomeric follistatin. It is tempting to speculate that prebinding of follistatin by heparin may serve as a mechanism to increase follistatin concentrations at the cell surface, providing a more efficient antagonism method than free floating follistatin. Therefore, it is important to consider how follistatin interacts with ligands in the context of the cell where differences in heparin/HS expression/sulfate patterning may mediate the interaction between follistatin and TGFβ ligands.

Numerous studies have attempted to use follistatin to block myostatin activity as a treatment for muscle wasting and cachexia pathologies. For example, insertion of follistatin into adeno-viral vectors has proven to be a potent method for localized anti-myostatin effects in both mice and non-human primates.[50] However, there are issues with bioavailability and turnover of FS. This is most likely due in part by follistatin being retained on the cell surface though heparin interactions. In fact, a recent study aimed at improving follistatin pharmacokinetics and pharmacodynamics showed that removal of the HBS within FS315 resulted in a substantial increase in its bioavailability.[51] This increase translated into a more potent follistatin molecule that aided in muscle recovery following cardiotoxin CTX muscle injury.[51] Therefore, an understanding of how follistatin binds heparin and how this impacts ligand binding is important to further develop these biologics.

Both heparin and HS are critical in modulating protein function in the extracellular environment. Though it is well known that heparin and HS interact with positively charged epitopes on the surfaces of proteins, the impact of this binding can be complicated and multifunctional. Here, we have shown that binding of heparin and HS to the TGFβ family antagonist not only allows it to bind to the cell surface but alters its ability to bind the ligands myostatin and activin A. This finding was unexpected and emphasizes that there is still much to learn regarding the interactions between proteins and heparin-like molecules.

AUTHORS' CONTRIBUTIONS

All authors participated in the design, interpretation of the studies, and analysis of the data, as well as review of the manuscript. R.G.W. and C.K. conducted the experiments; R.G.W., C.K., and E.J.G. compiled data and generated figures. R.G.W., E.J.G., and T.B.T. wrote the manuscript. F.Z. and R.J.L. provided study design and analysis. J.A.T. and R.J.L. assisted with data analysis.

DECLARATION OF CONFLICTING INTERESTS

The author(s) declared the following potential conflicts of interest with respect to the research, authorship, and/or publication of this article: R.G.W. is a co-founder, scientific advisor, and holds private equity in Elevian, a company that aims to develop medicines to restore regenerative capacity. Elevian provides sponsored research support to his past employer. T.B.T. is a consultant for Acceleron Pharma. The other authors declare no other conflicts.

ORCID iD

Thomas B Thompson (iD) https://orcid.org/0000-0002-7041-5047

REFERENCES

1. Yadin D, Knaus P, Mueller TD. Structural insights into BMP receptors: specificity, activation and inhibition. *Cytokine Growth Factor Rev* 2016;**27**:13–34
2. Ueno N, Ling N, Ying SY, Esch F, Shimasaki S, Guillemin R. Isolation and partial characterization of follistatin: a single-chain Mr 35,000 monomeric protein that inhibits the release of follicle-stimulating hormone. *Proc Natl Acad Sci U S A* 1987;**84**:8282–6
3. Otsuka F, Moore RK, Iemura S, Ichiro Ueno N, Shimasaki S. Follistatin inhibits the function of the oocyte-derived factor BMP-15. *Biochem Biophys Res Commun* 2001;**289**:961–6
4. Gumienny TL, Padgett RW. The other side of TGF-*β* superfamily signal regulation: thinking outside the cell. *Trends Endocrinol Metab* 2002;**13**:295–8
5. Abe Y, Minegishi T, Leung PCK. Activin receptor signaling. *Growth Factors* 2004;**22**:105–10
6. Glister C, Kemp CF, Knight PG. Bone morphogenetic protein (BMP) ligands and receptors in bovine ovarian follicle cells: actions of BMP-4,

-6 and -7 on granulosa cells and differential modulation of smad-1 phosphorylation of follistatin. *Reproduction* 2004;**127**:239–54

7. Sidis Y, Mukherjee A, Keutmann H, Delbaere A, Sadatsuki M, Schneyer A. Biological activity of follistatin isoforms and follistatin-like-3 is dependent on differential cell surface binding and specificity for activin, myostatin, and bone morphogenetic proteins. *Endocrinology* 2006;**147**:3586–97

8. Amthor H, Nicholas G, McKinnell I, Kemp CF, Sharma M, Kambadur R, Patel K. Follistatin complexes myostatin and antagonises myostatin-mediated inhibition of myogenesis. *Dev Biol* 2004;**270**:19–30

9. Nakatani M, Takehara Y, Sugino H, Matsumoto M, Hashimoto O, Hasegawa Y, Murakami T, Uezumi A, Takeda S, Noji S, Sunada Y, Tsuchida K. Transgenic expression of a myostatin inhibitor derived from follistatin increases skeletal muscle mass and ameliorates dystrophic pathology in mdx mice. *FASEB J* 2008;**22**:477–87

10. Cash JN, Angerman EB, Kattamuri C, Nolan K, Zhao H, Sidis Y, Keutmann HT, Thompson TB. Structure of myostatin·follistatin-like 3: N-terminal domains of follistatin-type molecules exhibit alternate modes of binding. *J Biol Chem* 2012;**287**:1043–53

11. Thompson TB, Lerch TF, Cook RW, Woodruff TK, Jardetzky TS. The structure of the follistatin:activin complex reveals antagonism of both type I and type II receptor binding. *Dev Cell* 2005;**9**:535–43

12. Cash JN, Rejon CA, McPherron AC, Bernard DJ, Thompson TB. The structure of myostatin:follistatin 288: insights into receptor utilization and heparin binding. *EMBO J* 2009;**28**:2662–76

13. Shimonaka M, Inouye S, Shimasaki S, Ling N. Follistatin binds to both activin and inhibin through the common beta-subunit. *Endocrinology* 1991;**128**:3323–5

14. Inouye S, Ling N, Shimasaki S. Localization of the heparin binding site of follistatin. *Mol Cell Endocrinol* 1992;**90**:1–6

15. Sidis Y, Schneyer AL, Keutmann HT. Heparin and activin-binding determinants in follistatin and FSTL3. *Endocrinology* 2005;**146**:130–6

16. Innis CA, Hyvönen M. Crystal structures of the heparan sulfate-binding domain of follistatin. Insights into ligand binding. *J Biol Chem* 2003;**278**:39969–77

17. Lerch TF, Shimasaki S, Woodruff TK, Jardetzky TS. Structural and biophysical coupling of heparin and activin binding to follistatin isoform functions. *J Biol Chem* 2007;**282**:15930–9

18. Hashimoto O, Nakamura T, Shoji H, Shimasaki S, Hayashi Y, Sugino H. A novel role of follistatin, an activin-binding protein, in the inhibition of activin action in rat pituitary cells: endocytotic degradation of activin and its acceleration by follistatin associated with cell-surface heparan sulfate. *J Biol Chem* 1997;**272**:13835–42

19. Delbaere A, Sidis Y, Schneyer AL. Differential response to exogenous and endogenous activin in a human ovarian teratocarcinoma-derived cell line (PA-1): regulation by cell surface follistatin. *Endocrinology* 1999;**140**:2463–70

20. Sumitomo S, Inouye S, Liu XJ, Ling N, Shimasaki S. The heparin binding site of follistatin is involved in its interaction with activin. *Biochem Biophys Res Commun* 1995;**208**:1–9

21. Zhang F, Beaudet JM, Luedeke DM, Walker RG, Thompson TB, Linhardt RJ, Fumin Z, Beaudet Julie M, Leudeke DM, Walker RG, Thompson TB, Linhardt RJ. Analysis of the interaction between heparin and follistatin and heparin and follistatin-ligand complexes using surface plasmon resonance. *Biochemistry* 2012;**51**:6797–803

22. Putnam CD, Hammel M, Hura GL, Tainer JA. X-ray solution scattering (SAXS) combined with crystallography and computation: defining accurate macromolecular structures, conformations and assemblies in solution. *Q Rev Biophys* 2007;**40**:191–285

23. Walker RG, Czepnik M, Goebel EJ, McCoy JC, Vujic A, Cho M, Oh J, Aykul S, Walton KL, Schang G, Bernard DJ, Hinck AP, Harrison CA, Martinez-Hackert E, Wagers AJ, Lee RT, Thompson TB. Structural basis for potency differences between GDF8 and GDF11. *BMC Biol* 2017;**15**:19

24. Stamler R, Keutmann HT, Sidis Y, Kattamuri C, Schneyer A, Thompson TB. The structure of FSTL3·activin a complex: differential binding of N-terminal domains influences follistatin-type antagonist specificity. *J Biol Chem* 2008;**283**:32831–8

25. Cash JN, Angerman EB, Keutmann HT, Thompson TB. Characterization of follistatin-type domains and their contribution to myostatin and activin a antagonism. *Mol Endocrinol* 2012;**26**:1167–78

26. Cash JN, Angerman EB, Kirby RJ, Merck L, Seibel WL, Wortman MD, Papoian R, Nelson S, Thompson TB. Development of a small-molecule screening method for inhibitors of cellular response to myostatin and activin A. *J Biomol Screen* 2013;**18**:837–44

27. Walker RG, Angerman EB, Kattamuri C, Lee YS, Lee SJ, Thompson TB. Alternative binding modes identified for growth and differentiation factor-associated serum protein (GASP) family antagonism of myostatin. *J Biol Chem* 2015;**290**:7506–16

28. Conrad HE. Nitrous acid degradation of glycosaminoglycans. *Curr Protoc Mol Biol* 1995;**32**:17.22.1–5

29. Schuck P. Size-distribution analysis of macromolecules by sedimentation velocity ultracentrifugation and Lamm equation modeling. *Biophys J* 2000;**78**:1606–19

30. Brown PH, Schuck P. Macromolecular size-and-shape distributions by sedimentation velocity analytical ultracentrifugation. *Biophys J* 2006;**90**:4651–61

31. Dyer KN, Hammel M, Rambo RP, Tsutakawa SE, Rodic I, Classen S, Tainer JA, Hura GL. High-throughput SAXS for the characterization of biomolecules in solution: a practical approach. *Methods Mol Biol* 2014;**1**:245–58

32. Rambo RP, Tainer JA. Accurate assessment of mass, models and resolution by small-angle scattering. *Nature* 2013;**496**:477–81

33. Rambo RP. Resolving individual components in protein-RNA complexes using small-angle X-ray scattering experiments. *Methods Enzymol* 2015;**558**:363–90

34. Petoukhov MV, Franke D, Shkumatov AV, Tria G, Kikhney AG, Gajda M, Gorba C, Mertens HDT, Konarev PV, Svergun DI. New developments in the ATSAS program package for small-angle scattering data analysis. *J Appl Crystallogr* 2012;**45**:342–50

35. Šali A, Blundell TL. Comparative protein modelling by satisfaction of spatial restraints. *J Mol Biol* 1993;**234**:779–815

36. Schneidman-Duhovny D, Hammel M, Sali A. FoXS: a web server for rapid computation and fitting of SAXS profiles. *Nucleic Acids Res* 2010;**38**:540–4

37. Weinkam P, Pons J, Sali A. Structure-based model of allostery predicts coupling between distant sites. *Proc Natl Acad Sci U S A* 2012;**109**:4875–80

38. Schneidman-Duhovny D, Inbar Y, Nussinov R, Wolfson HJ. PatchDock and SymmDock: servers for rigid and symmetric docking. *Nucleic Acids Res* 2005;**33**:363–7

39. Schneidman-Duhovny D, Inbar Y, Nussinov R, Wolfson HJ. Geometry-based flexible and symmetric protein docking. *Proteins Struct Funct Genet* 2005;**60**:224–31

40. Pelikan M, Hura GL, Hammel M. Structure and flexibility within proteins as identified through small angle X-ray scattering. *Gen Physiol Biophys* 2009;**28**:174–89

41. Khan S, Gor J, Mulloy B, Perkins SJ. Semi-rigid solution structures of heparin by constrained X-ray scattering modelling: new insight into heparin-protein complexes. *J Mol Biol* 2010;**395**:504–21

42. Ruppert R, Hoffmann E, Sebald W. Human bone morphogenetic protein 2 contains a heparin-binding site which modifies its biological activity. *Eur J Biochem* 1996;**237**:295–302

43. Gandhi NS, Mancera RL. Prediction of heparin binding sites in bone morphogenetic proteins (BMPs). *Biochim Biophys Acta Proteins Proteomics* 2012;**1824**:1374–81

44. Capila I, Linhardt RJ. Heparin–protein interactions. *Angew Chem Int Ed* 2002;**41**:390–412

45. Bishop JR, Schuksz M, Esko JD. Heparan sulphate proteoglycans fine-tune mammalian physiology. *Nature* 2007;**446**:1030–7

46. Rambo RP, Tainer JA. Characterizing flexible and intrinsically unstructured biological macromolecules by SAS using the Porod–Debye law. *Biopolymers* 2011;**95**:559–71

47. Schneidman-Duhovny D, Hammel M, Tainer JA, Sali A. Accurate SAXS profile computation and its assessment by contrast variation experiments. *Biophys J* 2013;**105**:962–74

48. Nakamura T, Sugino K, Titani K, Sugino H. Follistatin, an activin-binding protein, associates with heparan sulfate chains of proteoglycans on follicular granulosa cells. *J Biol Chem* 1991;**266**:19432–7

49. Nolan K, Kattamuri C, Luedeke DM, Deng X, Jagpal A, Zhang F, Linhardt RJ, Kenny AP, Zorn AM, Thompson TB. Structure of protein related to DAN and Cerberus: insights into the mechanism of bone morphogenetic protein antagonism. *Structure* 2013;**21**:1417–29

50. Kota J, Handy CR, Haidet AM, Montgomery CL, Eagle A, Rodino-Klapac LR, Tucker D, Shilling CJ, Therlfall WR, Walker CM, Weisbrode SE, Janssen PML, Clark KR, Sahenk Z, Mendell JR, Kaspar BK. Follistatin gene delivery enhances muscle growth and strength in nonhuman primates. *Sci Transl Med* 2009;**1**:1–17

51. Datta-Mannan A, Yaden B, Krishnan V, Jones BE, Croy JE. An engineered human follistatin variant: INSIGHTS into the pharmacokinetic and pharmocodynamic relationships of a novel molecule with broad therapeutic potential. *J Pharmacol Exp Ther* 2013;**344**:616–23